Chapter 4

Electrical, Magnetic and Dielectric properties of cobalt doped barium hexaferrite $BaFe_{12-x}Co_xO_{19}$ (x=0.0,0.05,0.1,and0.2) Ceramic Prepared via Chemical route

Electrical, Magnetic and Dielectric properties of cobalt doped barium hexaferrite BaFe12-x CoxO19 (x=0.0, 0.05, 0.1, and 0.2) Ceramic Prepared via Chemical route

4.1. Introduction

Ferrite (Fe_xO_y, Fe_3O_4/Fe_2O_3) is usually referred as ceramic of ferromagnetic materials and it appeared dark brown or grey in colors. They are very hard and brittle in nature and can be prepared by mixing of various transition metal oxides or alkaline metal oxides with the ferric oxides along with high temperature heat-treatment [Mubarak *et al.* (2018), Yasemian *et al.* (2019)].These types of metal oxide nano-particles have great attention in recent years due to possession of their unique properties such as catalytic, magnetic, electrical, biological, and optical and used in various industrial applications [Tartaj *et al.* (2011)]. A new class of ferrites has been discovered in 1952, that contains permanent magnetic properties are known as hexagonal ferrites. The general formula of hexagonal ferrites is $MFe_{12}O_{19}$ (Where M= Ca^{+2}, Sr^{+2}, Pb^{+2}, Ba^{+2} etc.).The divalent cations having similar ionic radii to that of divalent oxygen ions, makes it promising hexagonal ferrites [Ashima *et al.* (2012)].Depending upon the basis of their crystal structure, hexagonal ferrites can be categorized in to six types such as, M ($BaFe_{12}O_{19}$), W ($BaMe_2Fe_{16}O_{27}$), Y($Ba_2Me_2Fe_{12}O_{22}$), Z ($Ba_3Me_2Fe_{24}O_{41}$), X($Ba_2Me_2Fe_{28}O_{46}$), and U-type ($Ba_4Me_2Fe_{36}O_{60}$), where Me indicates the transition cations such as Zn, Mn, Co, Mg, etc [Jasrotia *et al.* (2019)]. Among them, M-type barium hexaferrite ($BaFe_{12}O_{19}$) containing $BaO.6Fe_2O_3$ units is a ferromagnetic materials with the space group *P6₃/mmc* having magnetization along C-axis [Soman *et al.* (2013)]. It has been widely used in largest volume fraction of permanent magnetic materials due to their resistivity and higher permeability as well as low cost production and attracts the great attention towards electronic industry and technology in various types of applications such as credit-card stripes, small motors, high-density memories and low-loss microwave devices [Özgür *et al.* (2009), Iqbal *et al.* (2010), Martirosyan *et al.*

(2011), Hussain *et al.* (2011)]. Such type of materials are very stable and having excellent magnetic properties due to large crystalline anisotropy, high saturation magnetization, high Curie temperature as well as high intrinsic corecivity. However, in the recent years the continuous demands with improvements in magnetic properties of these materials have been developed for device application. Therefore, several efforts were carried out for modifying the desired properties by researchers and technologists to the substitutions of other divalent or trivalent ions in place of Ba^{+2} or Fe^{+3} ions in the crystal structure of $BaFe_{12}O_{19}$ materials [Mosleh *et al.* (2016)]. These substitutions have great effect on the magnetic and microwave properties of the barium hexaferrite materials due to change in the complex permeability [Sözeri *et al.* (2016)].Till date, several research work has been carried out for their synthesis and characterization on the substitution of magnetic and nonmagnetic ions such as, $BaMe_xIr_xFe_{12-2x}O_{19}$ (Me^{+2} = Co, Zn), $BaZn_xSn_xFe_{12-2x}O_{19}$, $BaCo_xRu_xFe_{12-2x}O_{19}$, $BaMe_xFe_{12-x}O_{19}$ (Me^{+3}=Al, Cr, Bi, Sc), $BaMe_xTi_xFe_{12-2x}O_{19}$ (Me^{+2}=Co, Zn, Mn) and $BaMe_xTi_xFe_{11.6-2x}O_{19}$ (Me^{+2}=Co, Zn)with the dopants ions having same number of unpaired of electron[Zhao *et al.* (2005)].These types of substitutions change their microstructure, enhancement of magnetic properties as well as absorbing performance of hexaferrites as reported in earlier literatures[Mahmood *et al.* (2015), Cao *et al.* (2014), Lu *et al.* (2014), Pan (2014)]. In the present study, we have synthesized $BaFe_{12-2x}Co_xO_{19}$ (BHFC) ceramic with the various compositions where x=0.0, 0.05, 0.1 and 0.2 via chemical method for improvement of their dielectric and magnetic properties without affecting of phase formations.

4.2. Experimental Procedure

4.2.1 Synthesis

The samples of $BaFe_{12-x}Co_xO_{19}$ (BHFC) having compositions (x = 0.0, 0.05, 0.1, and 0.2) prepared via chemical method. Analytical grade chemical were used for this synthesis, barium nitrate Ba $(NO_3)_2$ (99% Merck, India), iron nitrate Fe $(NO_3)_3.9H_2O$ (98% Merck, India) and Co $(NO_3)_2.6H_2O$ (97% Merck, India) were taken as starting materials with their stoichiometric ratio. The metals nitrates of Ba, Fe and Co mentioned in the above were dissolved in doubled distilled water and then calculated amount of citric acid ($C_6H_8O_7.H_2O$, 99% Merck, India) act as compexing agent as per equivalent to metal ions was also added for chelation of Ba^{+2}, Fe^{+3}, Co^{+2} ions .

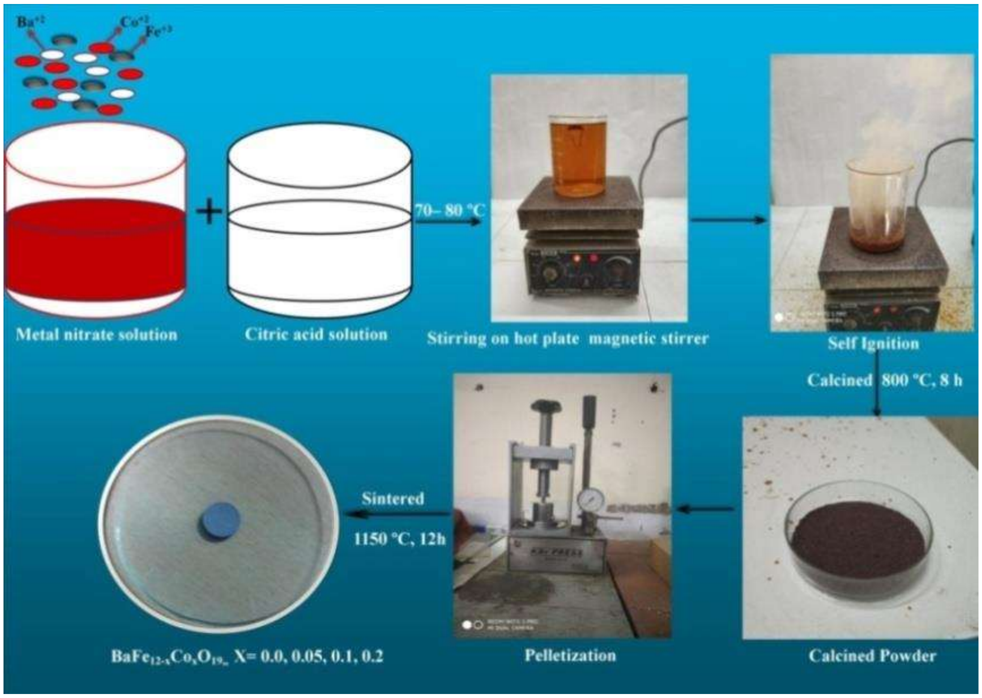

Figure 4.1 Experimental procedure for synthesis of $BaFe_{12-x}Co_xO_{19}$ (x= 0.0, 0.05, 0.1 and 0.2) ceramic via chemical route

The resulting solution was dried on the hot plate magnetic stirrer at 70-80 ºC for obtaining BHFC powder after removal of water which brunt with the sooty flame. The synthesized resulting powder was ground and calcined at 800 ºC for 8 h, then make a cylindrical pellets of the dimensions (11.5 mm × 1.00 mm) by using PVA (act as a binder) and applying pressure of 5 tons with the help of hydraulic press. Finally, the pellets were sintered at 1150 ºC for 12 h in an electrical furnace at scanning rate of 4 °C/min and further carried out different types physio-chemical characterizations. The summarized synthesis procedure is given in the Figure 4.1.

4.2.2 Electrode Preparation:

Electrodes were prepared by mixing 5 mg of catalyst, 0.2 mL of 2-propanol, 15µL Nafion. 80µL of the homogeneous distribution was spread on the carbon paper and dried at 80 °C with the help of an oven. Copper wire was attached to the electrode with the help of silver glue which acted as a current collector.

4.2.3. Characterization

The crystalline phase of the synthesized material ($BaFe_{12-x}Co_xO_{19}$, where x= 0.0, 0.05, 0.1, and 0.2) was identified by X-ray diffraction analysis (Rigakuminiflex 600, Japan) employing Cu-Kα radiation (λ=1.54 Å). The surface morphology, microstructure and elemental analysis of the BHFC were investigated by field emission scanning electron microscope (ZEISS, model EVO-18 research; Germany) and energy-dispersive X-ray spectroscopy, EDX (Oxford instrument; USA) respectively. Transmission electron microscope (TEM, FEI TECANI G^2 20 TWIN; USA) was used for particle size determination. The surface morphology of BHFC ceramic was examined by atomic force microscopy (NTEGRA Prima, Germany). Magnetic behaviors and temperature dependence Zero field cooling (M^{ZFC}), field cooling (M^{FC}) over a temperature range 5–300 K and applied a magnetic field ± 2 T were recorded by Quantum Design MPMS-3 and SQUID VSM dc magnetometer respectively. Dielectric and electrical measurement of the sample were carried out using polished and silver coated pellets that dried over 200 °C for 15 min and cooled naturally to room temperature. The frequency and temperature dependence dielectric properties of BHFC ceramic were carried out using an impedance analyzer (PSM 1735, NumetriQ 4th Ltd. U.K.).

4.2.4. Cyclic Voltammetry (CV) and Electrochemical Impedance Spectroscopy (EIS) characterization:

Electrochemical measurements of the electrodes were executed by cyclic voltammetry (CV) and Electrochemical Impedance Spectroscopy (EIS) techniques with the help of VersaSTAT 3instrument. Three electrode systems were chosen to study the electrochemistry of the prepared samples. Three electrode systems have the working electrode (active material of 2 mg), a counter electrode (Platinum) and a reference electrode (Ag/AgCl). Electrochemical impedance spectroscopy (EIS) took place at AC voltage amplitude of 10 mV within the frequency range of 100 kHz to 0.01 Hz. 1M KOH solution was used as an electrolyte for the electrochemical characterizations.

4.3. Results and discussion

4.3.1. Microstructural studies

Figure 4.2 exhibits the X-ray diffraction (XRD) patterns of $BaFe_{12-x}Co_xO_{19}$ (BHFC) ceramic of the compositions(x= 0.0, 0.05, 0.1, and 0.2) sintered at 1150 °C for 12 h. The phase formation of the hexagonal ferrite for all compositions is confirmed with the help of Joint Committee on

Powder Diffraction Standards (JCPDS cord- 78-0132) with space group *P6₃/mmc*. The phase formation of hexagonal ferrite at higher sintering temperature proceeds through the following reaction mechanism,

$$4[Fe(NO_3)_3.9H_2O] \rightarrow 2Fe_2O_3 + 12HNO_3 + 30H_2O \quad (4.1)$$

$$2Ba(NO_3)_2 \rightarrow 2BaO + 4NO_2 + O_2 \quad (4.2)$$

$$2Fe_2O_3 + 2BaO \rightarrow 2BaO.Fe_2O_3 \quad (4.3)$$

$$BaO.Fe_2O_3 + 5Fe_2O_3 \rightarrow BaO.6Fe_2O_3 \quad (4.4)$$

The intermediate product occurs in the reaction is monoferrite BaO. Fe_2O_3 [Ram (1989)]. However, at higher substitution of Co (x = 0.2) at iron site in barium hexaferrite, the minor secondary phase of Fe_2O_3 ($2\theta = 28.74°$) is also observed in the XRD pattern [Anupama *et al.* (2017), Choudhary *et al.* (2020), Choudhary *et al.* (2018) (a), Choudhary *et al.* (2017) (a), Choudhary *et al.* (2017) (b), Choudhary *et al.* (2018) (b)], confirmed with JCPDS Card No- 78-0132. As minor secondary phase of hematite (α-Fe_2O_3) is obtained from thermal decomposition of iron nitrate mentioned in the chemical reaction (Eq.4.1) does not directly react with the barium nitrate to form barium hexaferrite during the calcinations process. Then barium nitrate decomposes at higher temperature to form barium oxide, nitrogen dioxide and oxygen. Furthermore, the large proportions of Fe_2O_3 reacted with barium oxide to form barium hexaferrite with the small fraction of hematite (α-Fe_2O_3) residue as in the case of higher concentration of cobalt doping $BaFe_{12-x}Co_xO_{19}$ (x = 0.2) at sintering temperature 1150 °C for 12 h[Rusianto *et al.* (2015), Anantharamaiah *et al.* (2020), Anupama *et al.* (2017), Choudhary *et al.*

(2020), Choudhary *et al.* (2018) (a)].The peaks of the parent compound and doping substituents appear at the same positions with different intensities and full width at half maximum (FWHM) may be due to the occupation of substituted ions at crystallographic sites of Fe^{+3} ions [Vaishali *et al.* (2014)].

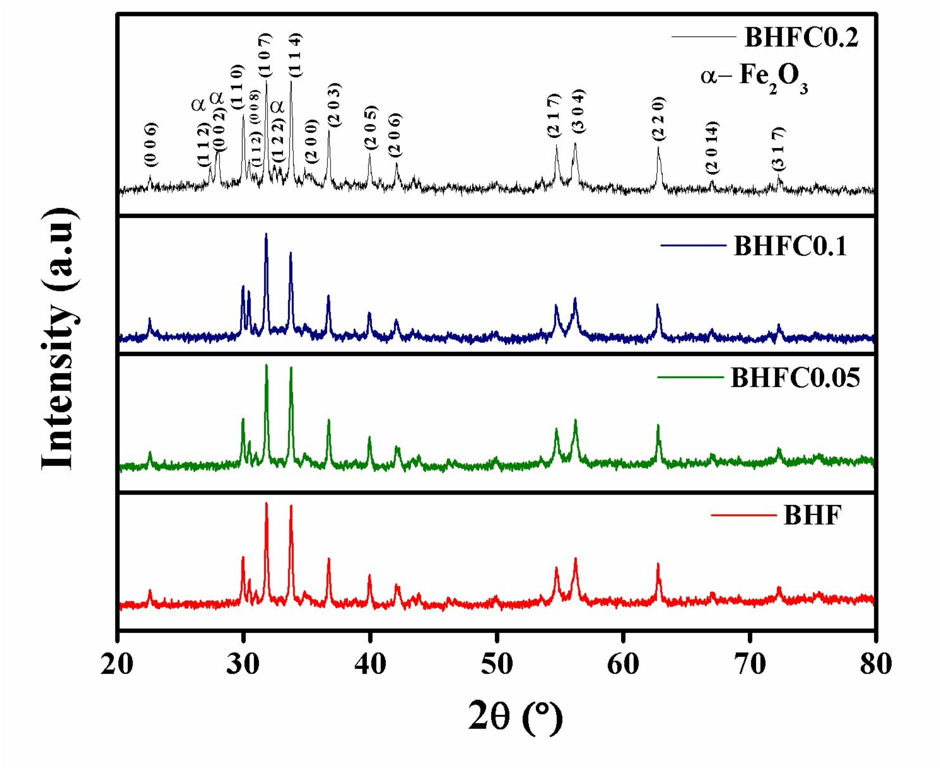

Figure 4.2 Shows XRD diffraction patterns of BHFC ceramic sintered at 1150 °C for 12 h.

The average crystallite size, *D* of BHFC ceramic was calculated by using the Debye Scherer formula [Kumar *et al.* (2019)].

$$D = \frac{k\lambda}{\beta \cos\theta} \tag{4.5}$$

where, D is the crystallite size, k is a constant whose value taken as 0.96, λ is the wavelength of radiation, θ is the Bragg angle of strongest intense peaks. β represents peak width of the diffraction peak at half-maxima (FWHM) in radians and it is corrected value of diffraction peak due to instrumental broadening for crystallite size with reference to standard silicon wafer sample. The average crystallite size of BHFC ceramic is calculated with the help of five most intense peaks and listed in table 4.1.

Le-Bail full pattern matching analysis is carried out for X-ray diffraction (XRD) patterns of $BaFe_{12-x}Co_xO_{19}$ (x = 0.0, 0.05, 0.1, and 0.2) ceramic is shown in Figure 4.3.

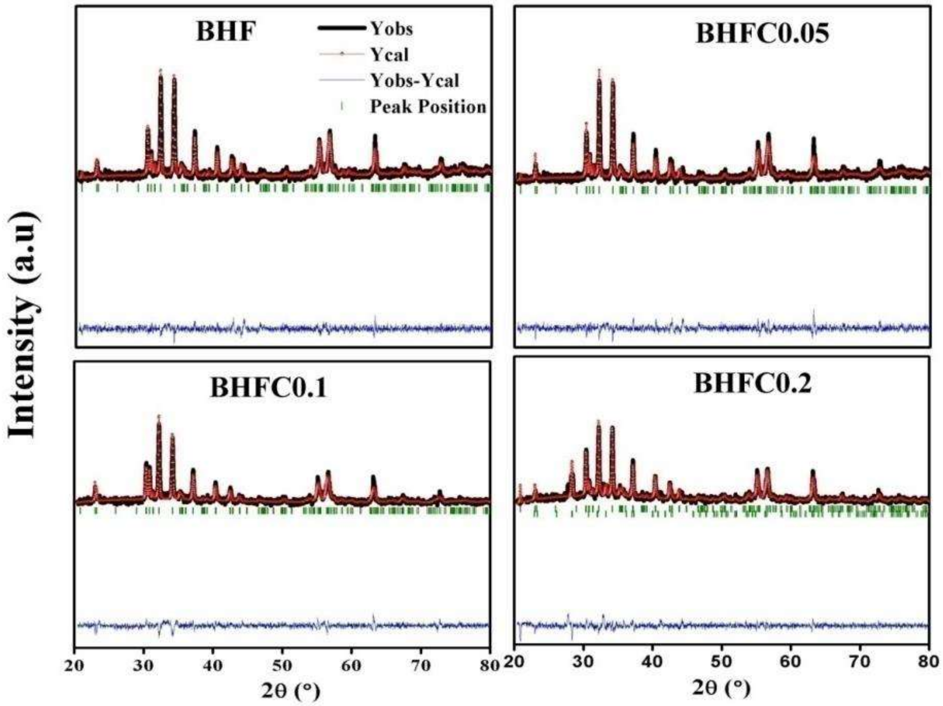

Figure 4.3 Le-Bail full pattern matching analysis of XRD patterns for $BaFe_{12-x}Co_xO_{19}$ (BHFC) ceramic with compositions x= 0.0, 0.05, 0.1, and 0.2 sintered at 1150 °C for 12 h.

The calculated pattern assigned as red color circle exactly overlapped with the observed pattern (black color circle) sustaining the good fitting of the XRD patterns. Goodness of fitting for all the samples was also confirmed with the low value of χ^2. All the observed Bragg's peaks confirm the presence of hexagonal symmetry with the space group *$P6_3/mmc$* [Kumar *et al.* (2017)] . There is no impurity phases were observed in the XRD pattern for the samples having compositions up to 0.1.

Table 4.1: Lattice parameters, crystal structures, angles, Bragg R-factor and RF-factor for $BaFe_{12-x}Co_xO_{19}$ (x = 0.0, 0.05, 0.1, 0.2) Ceramic.

Phase 1: $BaFe_{12}O_{19}$, Space group: P6$_3$*/mmc,* Angle: α = β = 90°, γ =120°, Hexagonal

Phase 2: α-Fe_2O_3 Space Group: Pna2$_1$ Angle: α = β = γ = 90°, Tetragonal

Samples			Lattice parameters (Å)		Vcell (Å^3)	FWHM Parameters			Bragg R-factor	RF -factor
$BaFe_{12-x}Co_xO_{19}$	χ^2	Crystallize size (nm)	a = b	c		U	V	W		
X = 0.0	1.17	41.48	5.8845	23.1820	802.7312	0.06004	-0.02192	0.00625	2.145	2.197
X = 0.05	1.38	39.02	5.8837	23.1867	802.6737	0.82493	-0.24916	0.00689	2.204	2.089
X = 0.1	1.49	35.99	5.8833	23.1852	802.5109	1.00401	-0.25258	0.00710	1.753	1.811
X= 0.2	1.77	33.56	5.8813	23.2002	802.4877	0.04535	-0.03393	0.00625	1.548	1.039
α-Fe_2O_3	–	–	7.6191	5.5879	324.3814	0.56443	-0.05201	0.15922	5.941	2.072

However, a small impurity peak of α-Fe_2O_3 phases is identified in the XRD pattern of the composition, x=0.2 which reveals the higher doping of cobalt in the barium hexaferrite has not been considered for further analysis due to presence of secondary phase of α-Fe_2O_3 after x= 0.1[Buzinaro *et al.* (2016)].The refined value of lattice parameter, angles, unit cell volume, FWHM parameters, Bragg R-factor and RF-factor for all the compositions of BHFC ceramic were also listed in table 4.1.

The variation in lattice parameters of cobalt substituted barium hexaferrite with cobalt concentrations (x= 0.0, 0.05 0.1, and 0.2) is shown in Figure 4.4a.

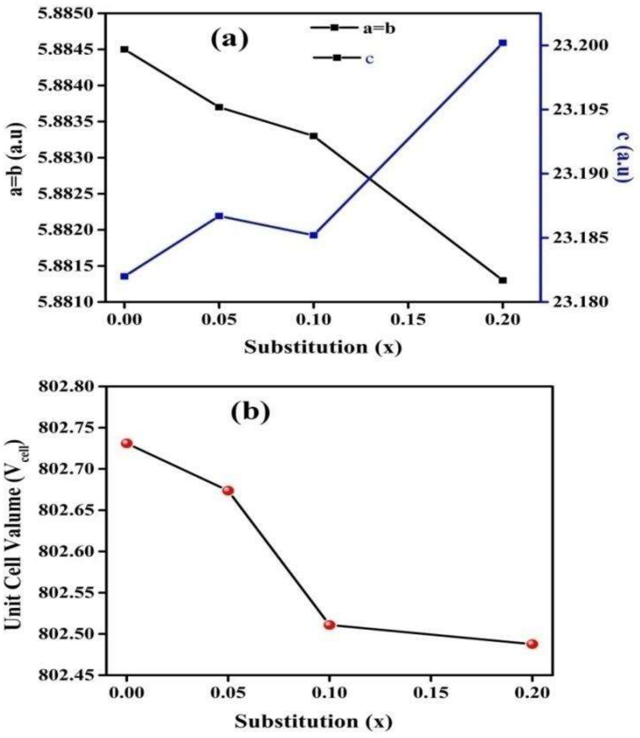

Figure 4.4 (a) Variation of lattice parameters a = b and c with cobalt concentration (x = 0.0, 0.05, 0.1, and 0.2). (b) Variation of unit cell volume with cobalt concentration (x = 0.0, 0.05, 0.1, and 0.2) of $BaFe_{12-x}Co_xO_{19}$ ceramic.

It is observed from the figure that the value of lattice parameter (*a* =*b*) linearly decreases with increasing Co concentrations from 0.0 to 0.2, while the value of *c* linearly increases with increasing concentration of cobalt. The decreasing and increasing value of lattice parameters *a* and *c* are good agreements with the Shannon- Prewitt crystal radius and confirmed the success substitution of Co^{+2} (r_{Co} = 0.61 Å) ions at Fe^{+3} (r_{Fe}= 0.64 Å) ions sites for formation of $BaFe_{12-x}Co_xO_{19}$ [Mallick *et al.* (2007), You *et al.* (2019), Tran *et al.* (2018)].The variation of unit cell volume with Co concentration of the barium hexaferrite ceramic is depict in Figure 4.4b which reveals that unit cell volume (V_{cell}) starts decreases with increasing concentrations of Co which is due to the smaller ionic radii of substituted Co^{+2} (0.61 Å) than Fe^{+3} (0.64 Å) confirmed the successive substitution of Co^{+2} in $BaFe_{12}O_{19}$ [Arora *et al.* (2016)].

Fourier-transform infrared (FTIR) spectrograms of cobalt doped barium hexaferrite (BHFC) ceramic measured from the wavelength 400 - 4000 cm^{-1} are depicts in Figure 4.5. All the peaks corresponding to all synthesized materials revealed the same IR absorption behavior. The presence of absorptions bands at 447, 503, 543, 591 cm^{-1}as shown in inset of figures 4.5 and 751 cm^{-1} are due to the out of plane of bending and asymmetric Fe-O stretching vibration bands of octahedral and tetrahedral sites, respectively in the BHFC ceramic. The metal-oxygen bonds of Ba-O also appear at 895 cm^{-1} and the broad absorption bands at 1630 and 3440 cm^{-1} are related to OH functional group in the moist atmosphere. The IR peaks observed in the range of 1000-1500 cm^{-1} represented by the circle reveals the presence of metal-Oxygen-Metal such as Fe–O–Fe or Co-O-Co bands in BHFC ceramic. All the absorption bands in the FTIR spectrum confirm the formation of hexaferrite [Gordani *et al.* (2014)].

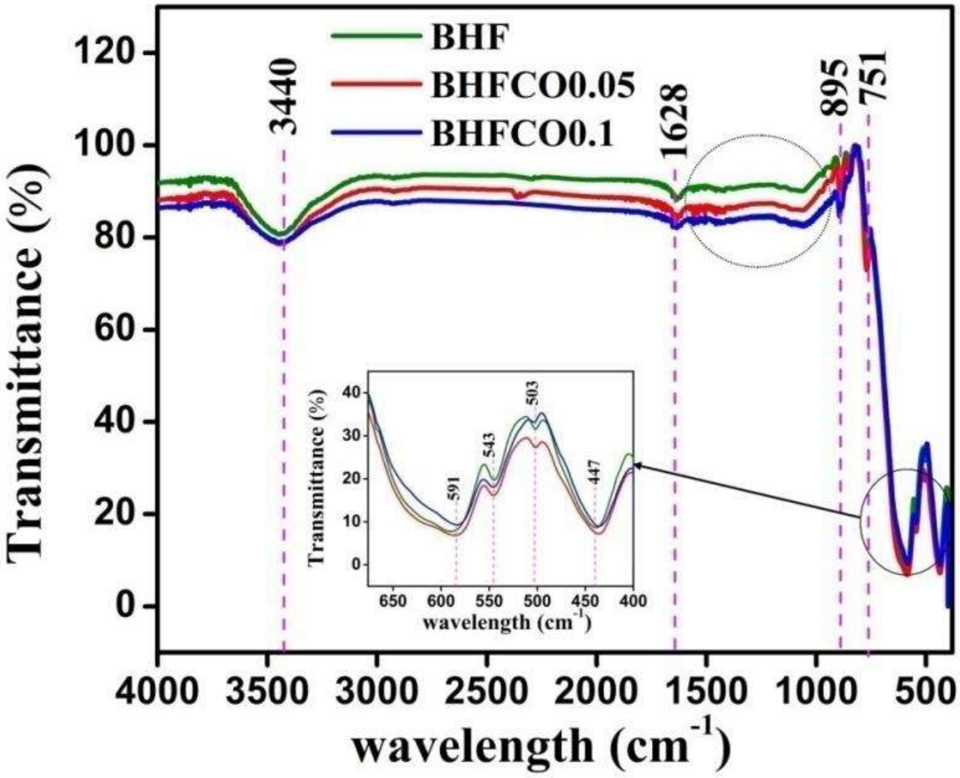

Figure 4.5 FTIR spectra of BHFC ceramic sintered 1150 °C for 12 h.

The surface morphological observation of the cobalt doped barium hexaferrite having the composition (x = 0.0, 0.05 and 0.1) was performed by using bright field transmission electron microscopy (TEM) studies as shown in Figure 4.6a. The results shows the hexagonal and rod shape of the particles having particle size 213, 185 and 52 nm, respectively on the scale of 100 nm (histogram not shown here) which clearly reveals that the size of the BHFC ceramic particle decreases with increasing Co^{+2} concentrations. Figure 4.6b shows the selected area diffraction (SAED) patterns of BHFC ceramic.

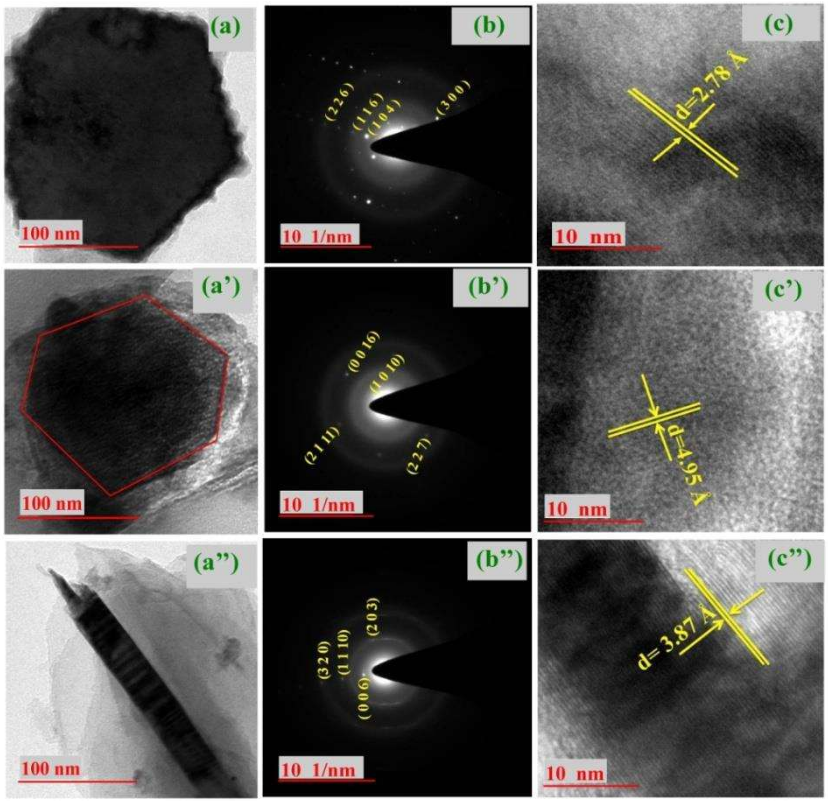

Figure 4.6 (a) Bright field TEM image (**b**) selected area diffraction (SAED) pattern (**c**) High-resolution TEM image of BHFC ceramic sintered 1150 °C for 12 h.

All the diffraction patterns observe in SAED patterns for different compositions possess through the distinct planes. The zone axis [*U V W*] obtained for all compositions in between the planes (1 1 6) and (1 0 4), (1 0 10) and (2 1 11), (3 2 0) and (2 0 3) are $[4\ \bar{2}\ \bar{1}]$, $[\overline{10}\ \bar{9}\ 1]$, $[6\ 9\ \bar{4}]$, respectively. High resolution transmission electron microscopy (HR-TEM) image of the synthesized BHFC ceramic is shown in Figure 4.6c. Inter-planer (*d*) spacing obtained by HR-TEM is 2.78 Å (100 %), 4.95 Å (12 %), 3.87 (11 %) corresponding to the planes (1 0 7), (1 01) and (0 0 6) for the composition x = 0.0, 0.05, and 0.1, respectively. The entire planes of SAED pattern and HR-TEM are also well matched with the above mentioned XRD results (JCPDS card No: 27-1029) [Kumar *et al.* (2019)].

High resolution scanning electron microscopy (HR-SEM) images of gold plated fractured surface of pellets of cobalt doped barium hexaferrite (x = 0.0, 0.05 and 0.1) is depicted in Figure 4.7 a, c, and d, respectively on the 500 nm scale.

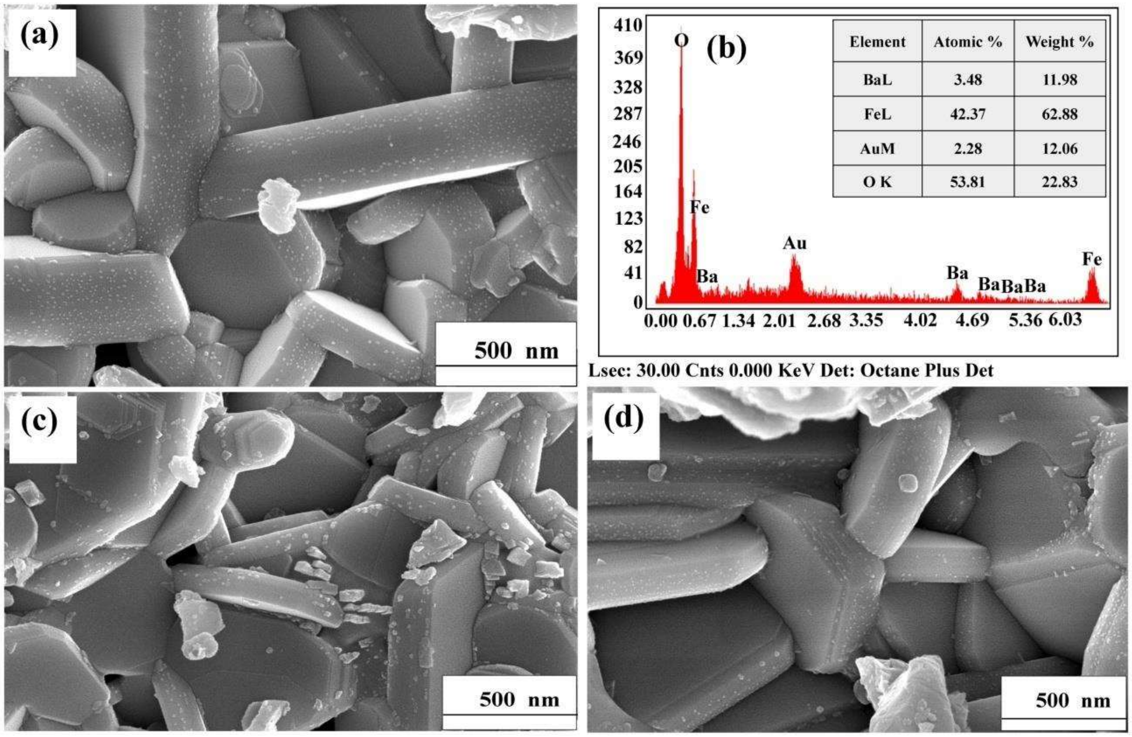

Element	Atomic %	Weight %
BaL	3.48	11.98
FeL	42.37	62.88
AuM	2.28	12.06
O K	53.81	22.83

Figure 4.7 (a, c and d) indicates SEM image with compositions x= 0.0, 0.05, and 0.1 **(b)** EDX spectra of BHFC ceramic at x=0.0 sintered at 1150 °C for 12 h.

The figures reveal the morphology of hexagonal plate-like shape of the grains with high aspect ratio that appear to grow along c-axis direction. The decreasing aspect ratio of barium hexaferrite is obtained on the substitution in BHFC ceramic. A larger growth of the grains with hexagonal structure were observed for the cobalt doped BHF ceramic with the composition x = 0.1. The average grain size of BHFC ceramic was calculated by using image J software and found to be 0.50, 0.84 and 1.0 μm for the compositions (x = 0.0, 0.05 and 0.1), respectively. These results indicate that average grain increases with increasing the concentrations of Co^{+2} in BHFC ceramic [Tanwar *et al.* (2018)]. Moreover, the average crystallite size and particle size calculated by XRD and TEM measurement is smaller than average grain size obtained by HR-SEM which infer that the each particle is formed due to agglomeration of several crystallites and formation of crystallite due to combination of few particles. Figure 4.7b indicates the energy-dispersive X-ray spectroscopy (EDX) spectrum of BHFC ceramic with the composition x = 0.0 sintered at 1150 °C for 12 h. The presence of Ba, Fe and O elements inferred from EDX spectra with the atomic and weight percentage are shown in inset of the figure 4.7b, confirm the stoichiometric and purity of the synthesized materials.

The microstructure of fractured surface observed by atomic force microscopy (AFM) analysis for BHFC (x = 0.1) ceramic sintered at 1150 °C for 12 h is depicted in Figure 4.8. A clear grains with bimodal structure which separated by grain boundaries were observed in the materials by two dimensional (2D), AFM image as shown in Figure 4.8a. The value of amplitude parameters such as Maximum height of the profile (R_{max}), Maximum profile peak height (R_p) and Maximum profile valey depth (R_v) observed by 2D AFM analysis are 2.218, 0.943 and 1.274 μm on the scanned area 20 × 20 mm^2.

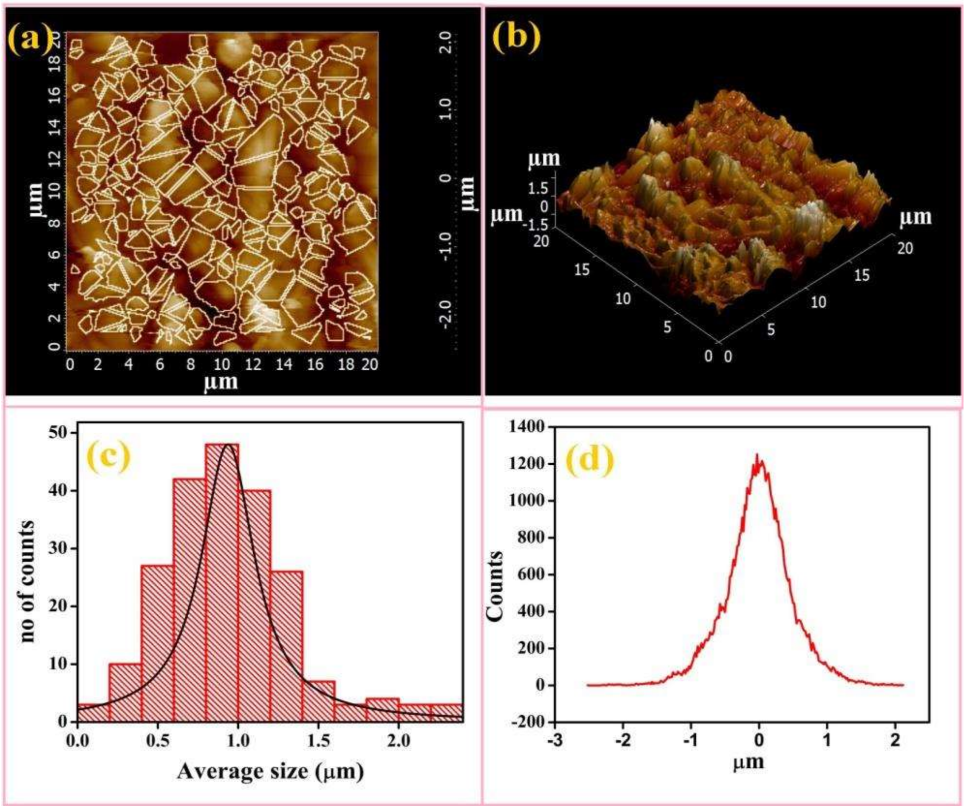

Figure 4.8 AFM images of BHFC ceramic at compositions x = 0.1 **(a)** two dimensional image for grain boundary (**b)** three dimensional for surface roughness (**c)** depth histogram graph and **(d)** bar diagram for particle size distribution.

The surface roughness (S_a) of the three dimensional AFM images are calculated and found to be 0.368 µm on same scanned area is mentioned in Figure 4.8b. The average grain size of BHFC ceramic obtained by Histogram plots for 2D AFM image are found to be 600 nm which are comparable with the SEM results, is mentioned in Figure 4.8c. Figure 4.8d indicates peak distribution curve of 3D AFM image emphasized the surface roughness of the BHFC ceramic.

4.4. Ferroelectric Measurements

Figure 4.9 depicts the ferroelectric characteristics of BHFC with compositions(x = 0.0, 0.05 and 0.1) were measured by the polarization-electric field (P-E) hysteresis loops at room temperature and at frequency of 50 Hz under the applied electric field 6 kV/cm.

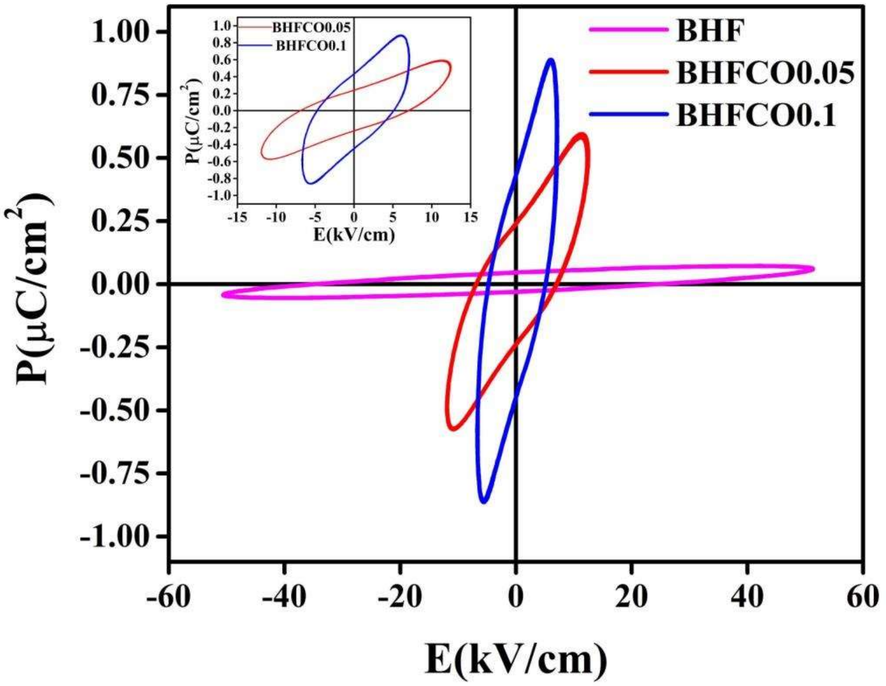

Figure 4.9 The polarization verses Electric field (P–E) hysteresis loop of BHFC ceramic at room temperature for compositions x = 0.0,0.05 and 0.1.

The figure reveals that the value of remnant polarization (P_r) and coercivity (E_c) increases and decreases, respectively with increasing the concentrations of cobalt ion (Co^{+2}).The remnant polarization (P_r) and coercivity (E_c) values for all compositions were listed in table 4.2. It is observed that from table, the value of remnant polarization (P_r) for the composition x = 0.1 is found to be higher than other compositions (x = 0.0, 05) suggesting that increasing ferroelectric properties of the BHFC ceramic [Hoque *et al.* (2018)]. Furthermore, no saturation polarization is observed in P-E hysteresis curve which indicates lossy characteristics of the materials.

Table 4.2 Remnant polarization (P_r) and Coercivity (E_c) of BHFC (x = 0.0, 0.05, and 0.1) ceramic at room temperature.

compositions (x)	Remnant polarization (μC/cm^2)	Coercivity (kV/cm)
BHF	0.048	23.803
BHFCO0.05	0.239	9.170
BHFCO0.1	0.441	4.928

4.5. Dielectric properties

The dielectric study of synthesized material is one of the significant characterizations which provide the information about dielectric constant (ε) as well as dielectric loss (tan *δ*) along with the specific orientations in presence of electric fields at the operated frequency with the temperature. The parameters related with the dielectric were investigated through high precision multimeter attached with temperature control (furnace) and a computer set up. The dielectric constant and dielectric loss of synthesized materials can be measured from collecting capacitance data with the help of general expressions at a particular temperature and a frequency.

$$\varepsilon = \frac{C \times l}{\varepsilon_0 \times A} \tag{4.6}$$

where, C, l, A are the capacitance, thickness and area of the cylindrical pellets and ε_0 is the permittivity of free space (8.85 × 10^{-12} Fm^{-1}). The dielectric constant and dielectric loss of BHFC ceramic having compositions(x = 0.0, 0.05 and 0.1) as a function of temperature at 100 Hz is shown in Figure 4.10a and b.

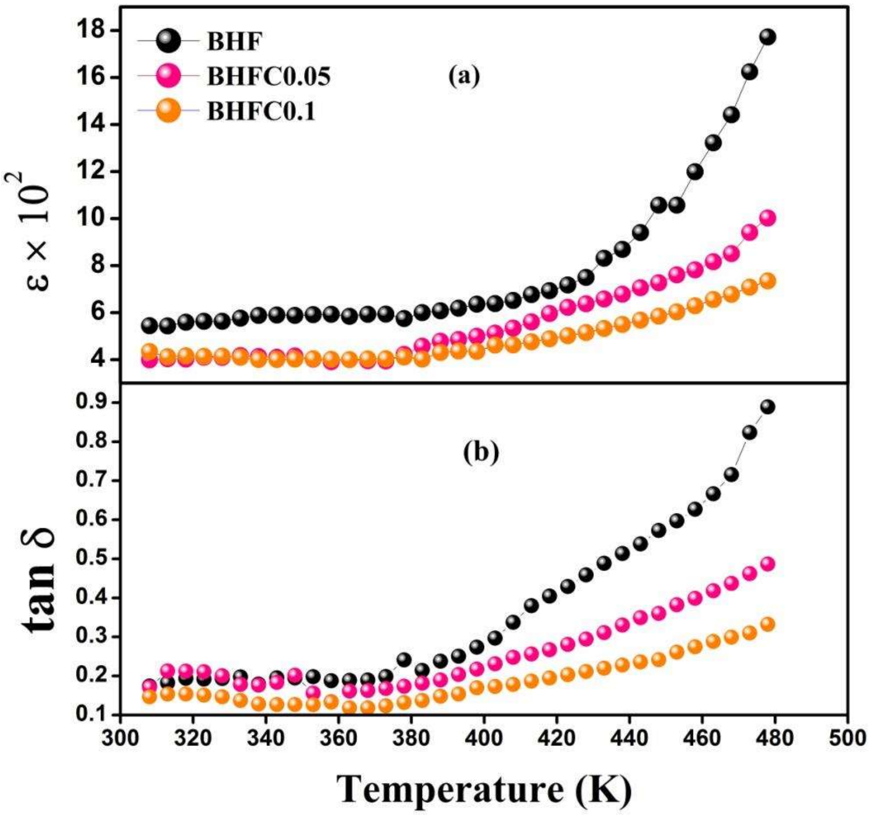

Figure 4.10 The variation of **(a)** Dielectric constant (ε) and **(b)** dielectric loss (tan δ) with temperatures at few selected frequencies for BHFC ceramic sintered at 1150 °C for 12 h.

It is observed from the figure that both of dielectric constant and dielectric loss value decreases with increasing concentration of cobalt substitution. The value of ε and tan δ at constant frequency (100 Hz) obtained from the plots are found to be 1.7 × 10^3 and 0.9, respectively of cobalt doped barium hexaferrite (BHFC) ceramic. The high value of ε and low value of tan *δ* with temperature is due to orientation of dipoles with the electric field which facilitates to enhance the space charge polarization arises from the difference of conductivity in the materials [Yadava *et al.* (2017)].

Frequency dependent dielectric constant (ε) and dielectric loss (tan *δ*) of cobalt substituted barium hexaferrite (BHFC) ceramic at room temperature is depicted in the Figure 4.11.

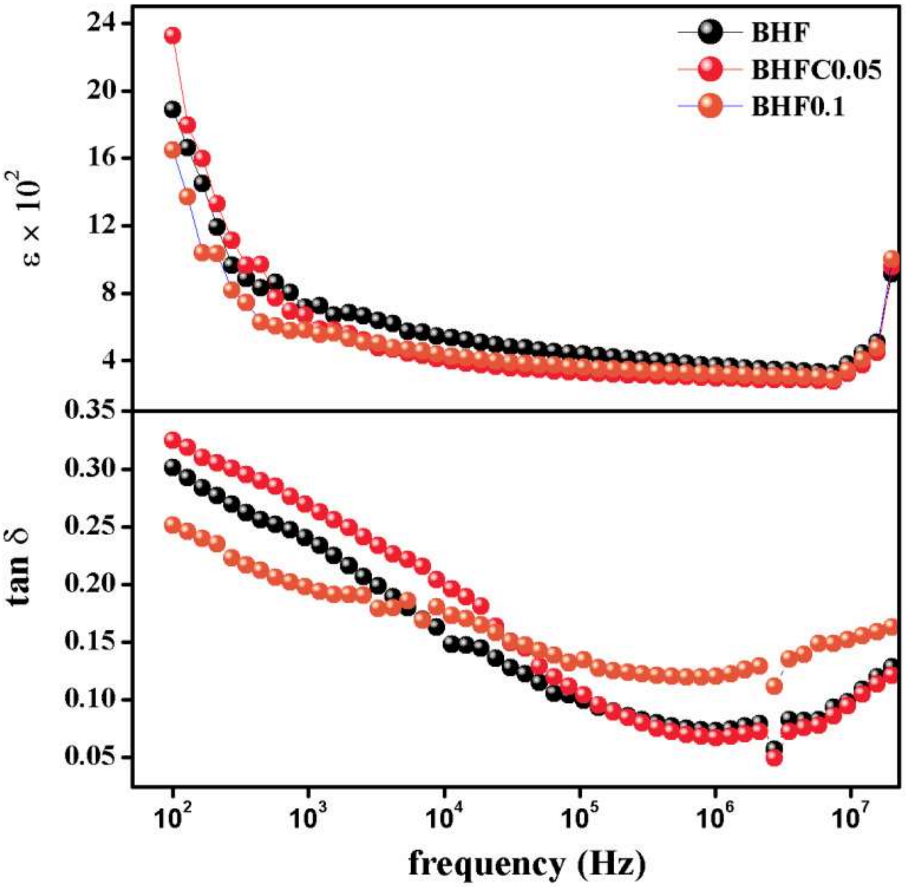

Figure 4.11 Frequency dependent **(a)** dielectric constant (ε') and **(b)** dielectric loss (tan δ) at few selected temperatures of BHFC ceramic.

The continuous decrease in ε is observed in the low frequency region from 100 – 1 kHz and slowly decreases after 1 kHz in the high frequency region. The decrease in dielectric constant with the frequency is due to grains and grain boundaries contribution. This can be explained that grains are semiconducting in nature, occurs predominantly at higher frequency side and grain boundaries are poorly conducting in nature which is more predominant in the lower frequency sides' results high value of dielectric constant of the materials. The value of ε and tan δ are calculated from the plots and found to be 2.3×10^3 and 0.32, respectively for concentration x= 0.05 at 100 Hz. It is observed that both the values (ε and tan δ) for concentration x = 0.05 higher than that of parent BHF and BHFC (x= 0.1). This abrupt change in the values of dielectric constant and dielectric loss of BHFC ceramic are mainly due to difference in grain size, morphology and density of the synthesized materials [Yadava *et al.* (2018), Bammannavar *et al.* (2009)].

4.6. Conductivity measurements

Frequency dependence of AC conductivity for BHFC ceramic for a few selected concentrations and at 303 K, temperature is shown in Figure 4.12. According to the Almond–West type power law, the total conductivity(σ) of the BHFC ceramic is calculated by the Eq. 4.7.The frequency dependent of AC conductivity for the material is analyzed by the Jonscher's power law as shown in Eq. 4.8.

$$\sigma = \sigma_{dc} + \sigma_{ac} = \sigma_{dc} + A\omega^s \qquad (4.7)$$

$$\sigma_{ac} = A\omega^S \qquad (4.8)$$

where, *s* is the frequency exponent factor which depends on the temperature as well as the compositions and its value in the range of 0 and 1.This factor is useful to differentiate the electrical conduction mechanism arises due to interaction of charge carriers in different material. σ_{ac} is ac conductivity dominant in lower frequency and higher temperature that arises due to hopping charge at the octahedral sites of Fe^{+3} in the materials and σ_{dc} is the temperature dependent dc conductivity occurs due to free charge carriers. *A* is the pre-exponential factor, *ω* is angular frequency ($\omega = 2\pi f$) [Chauhan *et al.* (2012)].

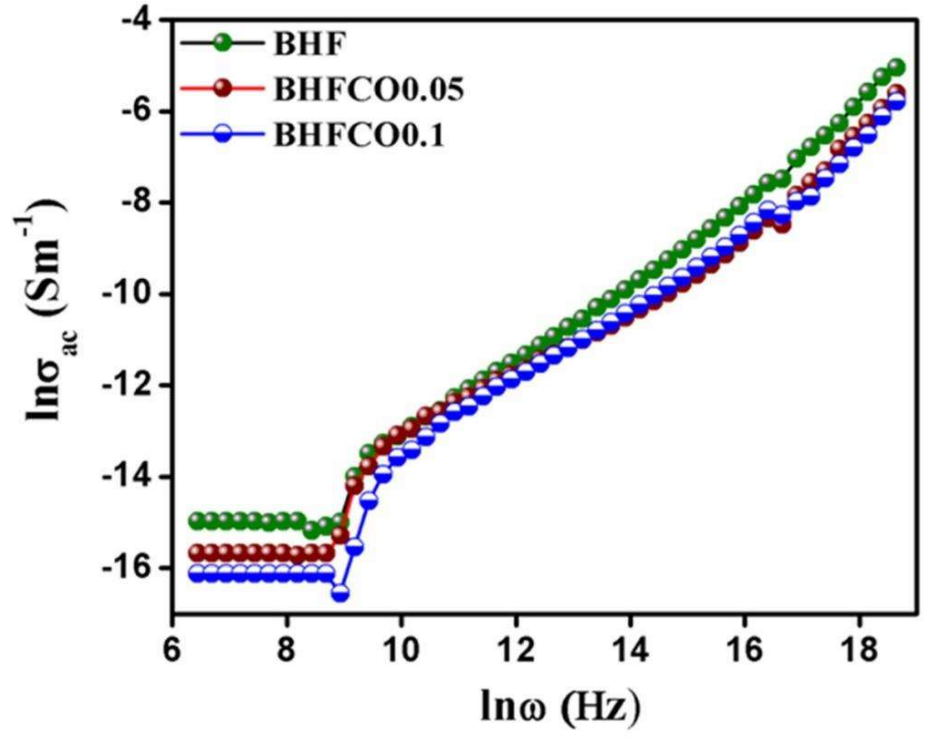

Figure 4.12 Frequency dependence of AC conductivity for BHFC ceramic for few selected concentrations and at 303 K temperature.

The value of *s* for BHFC ceramic calculated from the plot and found to be 1.23, 1.31 and 1.35, respectively for the concentration of Co^{+2} (x= 0.0, 0.05 and 0.1) at room temperature. The observed value of s from the plots for given concentrations are approximately equal to one. It is observed that the value of exponent parameter obtained by linear square fitting increases with increasing Co^{+2} concentration follows the opposite trends of the conductivity, related to the hopping charge conduction mechanism in the BHFC materials [Taher *et al.* (2015)].

Plots of conductivity with inverse of temperature at 100 Hz frequency of BHFC ceramic for certain concentrations are depicted in Figure 4.13.

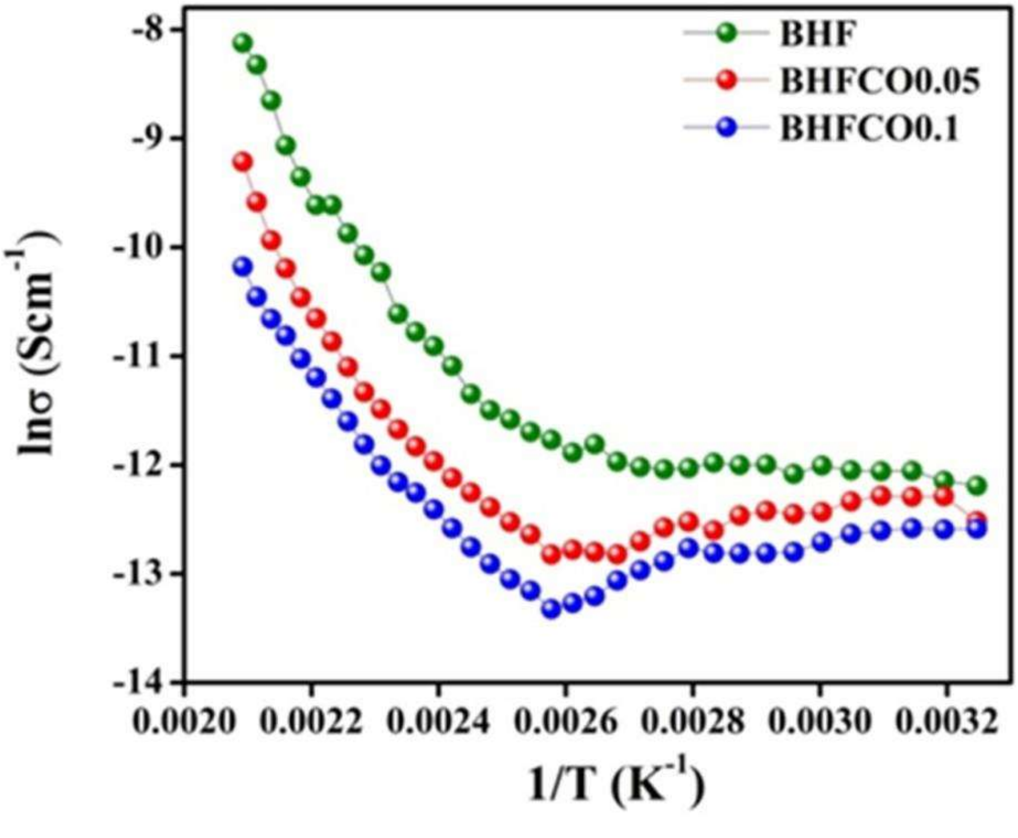

Figure 4.13 plots of AC conductivity with inverse of temperature Frequency for few selected concentrations and at 100 Hz frequency.

The temperature dependence of AC conductivity was strongly dominant at lower frequency region in comparison to higher frequency due to the existence of thermally activation process from the different localized state in the band gap [Okutana *et al.* (2005)].The temperature dependence of AC conductivity obeys the Arrhenius law, given by the following Eq.4. 9.

$$\sigma = \sigma_0 \exp(\frac{-E_a}{kT}) \tag{4.9}$$

where, E_a is the activation energy for the thermally activated process, σ_0 is the pre-exponential factor, k is the Boltzmann constant and T is the absolute temperature. The activation energy is calculated by the slope of the curves and found to be 0.120, 0.116, and 0.077 at 100 Hz for x= 0.0, 0.05 and 0.1, respectively. The activation energy of the BHFC ceramic is observed to be concentration dependent and decreases with increasing the doping concentration of Co. The linear decrease in activation energy with the composition due to increase in the charge carriers which enhance the conductivity of the synthesized materials [Ahmed *et al.* (1996)].

4.7. CV and EIS Result:

Cyclic voltammetry was performed to find out the current response of the prepared samples as shown in Figure 4.14a. The stability potential window for the prepared samples was taken as 1 volt and the potential scan rate was 20 mV/s. Sample with 0.1% doping of cobalt concentration has the highest current response, which demonstrates its better conductivity than the other samples. It can be observed that the current response decreases with the decrease in doping concentration and the bare sample BHFC has the least current response. From the EIS plot as shown in Figure 4.14b, it can be seen that the solution resistance for all the electrodes are almost same. The charge transfer resistance (diameter of the semicircle intersecting the real impedance axis) is decreasing with the increase doping concentration of Co^{+2}. This could be due to the increase in conductivity of the electrodes as the doping percentage increases. These results fit well with the cyclic voltammetry results (as sample doped with 0.1 % has the highest current response and the least resistance).

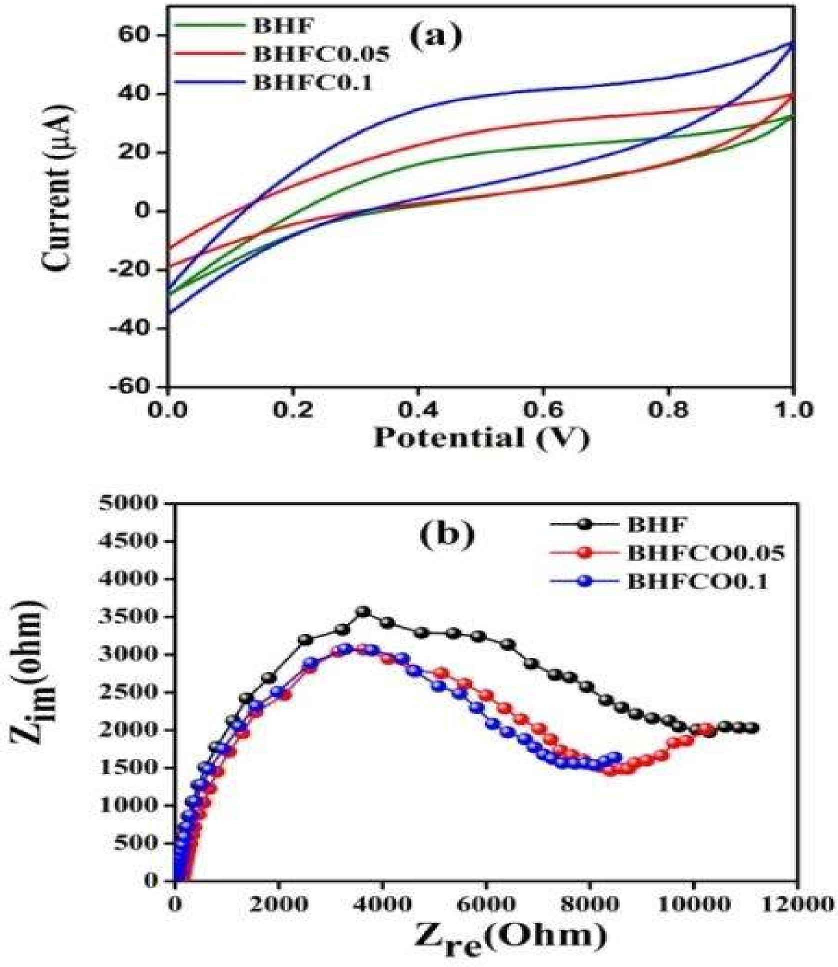

Figure 4.14 (a and **b)** show CV and EIS plots of BHFC ceramic sintered at 1150 °C for 12 h.

4.8. Magnetic studies

M-H hysteresis plots of BHFC ceramic with compositions x = 0.0, 0.05 and 0.1 were measured using vibrating sample magnetometer (VSM) at 100 K temperatures and magnetic field of ±2 *T* is depicts in Figure 4.15. It is emphasized from the figure that saturation magnetization (M_s) as well as remnant magnetization (M_r) terms decreases with increasing the cobalt concentration, However, the increase in coercivity (H_c) is observed increasing Co^{+2} substitutions in the barium hexaferrite. The value of saturation magnetization (M_s), remnant magnetization (M_r) as well as coercivity were calculated from the plots and are mentioned in table 4.3.

Table. 4.3. Magnetic parameters of $BaFe_{12-x}Co_xO_{19}$ ceramic with x = 0.0, 0.05, and 0.1.

Parameters	BHF	BHFC0.05	BHFC0.1
M_s (emu/g)	75.36	68.31	56.08
M_r (emu/g)	56.75	50.03	40.61
Hc (A/m)	2.73×10^5	2.79×10^5	3.49×10^5
$S_q = M_r/Ms$	0.753	0.732	0.724

The lower value of cobalt doped barium hexaferrite as compared to pure BHF, *Ms* =75.36 emu/g can be attributed to influence of fabrication conditions on the structural properties and the difference in their magnetic moment (Co^{+2} = 3 μB and Fe^{+3} = 5 μB). Furthermore, the preferential occupancies of Co^{+2} ions in the BHFC ceramic are known to be either 2b sites (ferromagnetically ordered) or antiferromagnetically ordered $4f_2$ sites [Chawla *et al.* (2014)]. The reduction in the value of *Ms* in case of BHFC ceramic as compared to pure BHF ceramic suggest that Co^{+2} ions are preferred in the 2b sites [SÖzeri (2009)].Furthermore, the value of H_c for pure BHF is found to be higher emphasized the higher value of magnetocrystalline anisotropy along c-axis. The decrease in the coercivity value with increasing cobalt concentrations are ascribed due to reduction in magnetocrystalline anisotropy [Kishimoto *et al.* (1987), Mendoza-Suarez *et al.* (2003)].The value of squareness ratio (S_q) calculated from the formula, $S_q = M_r/M_s$ and found to be 0.75, 0.73, 0.72 for x= 0.0, 0.05 and 0.1, respectively. The higher value of S_q ($M_r/M_s \geq 0.5$) explained that particles exist in the single magnetic domain which behaves as hard magnetic materials and useful in the fields of microwave devices, magnetic recording media, in multilayer chip inductors operating in GHz and high frequency electromagnetic devices [Mallick *et al.* (2007)].

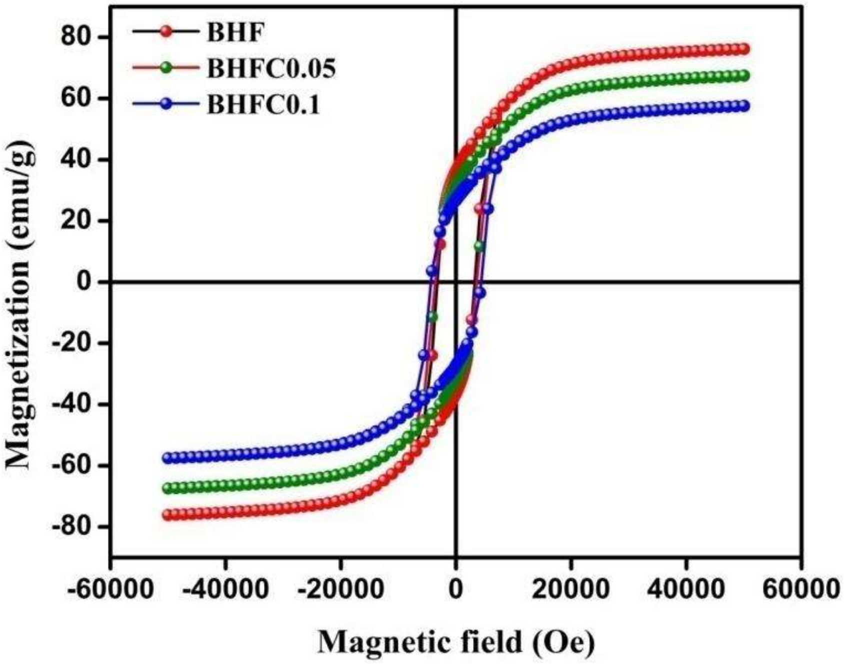

Figure 4.15 M-H hysteresis plots of BHFC ceramic with compositions x = 0.0, 0.05 and 0.1 sintered at 1150 °C for 12 h.

4.9. Conclusion:

In the present research work, $BaFe_{12-x}Co_xO_{19}$ (BHFC) hexaferrites with the composition (x = 0.0, 0.05, 0.1, and 0.2) were successfully synthesized by the chemical method using inexpensive metal nitrates at sintering temperature 1150 °C for 12 h. Single phase confirmation of the synthesized materials investigated through X-ray diffraction (XRD) analysis. SEM results confirmed the hexagonal nature of the grains in the size of 0.50, 0.84 and 1.0 µm for the compositions x= 0.0, 0.05, 0.1, respectively and also confirmed by TEM analysis with the particle size 213, 185 and 52 nm, respectively with respect to Co^{+2} concentrations. The value of ε and tan δ observed at certain frequency (100 Hz) are $2.3 \times 10^3$and 0.32, respectively of BHFC ceramic. The value of squareness (M_r/M_s) ratio for the synthesized BHFC ceramic are found to be 0.7 which indicates the single magnetic domain crystal structure of the hard magnetic materials that makes most suitable in the various field of ferrite core, sensors, permanent magnets for power generation, microwave absorbers for microwave darkroom, magnetic recording media, switch mode supplies and capacitor, in multilayer chip inductors operating in GHz and high frequency electromagnetic devices.